Journal of the Physical Society of Japan **91**, 044003 (2022)
https://doi.org/10.7566/JPSJ.91.044003

Bifurcation-Based Quantum Annealing with Nested Spins

Kazutaka Takahashi

Institute of Innovative Research, Tokyo Institute of Technology, Yokohama 226-8503, Japan

(Received January 28, 2022; accepted February 8, 2022; published online March 8, 2022)

We study a bifurcation mechanism of quantum annealing. Using spins with quantum number $S = 1$, we construct a simple model to make a bifurcation. The qutrit can be composed by nesting two qubits. We numerically solve the Schrödinger equation to confirm that the bifurcation-based quantum annealing (BQA) works well and the ground state can be found efficiently. The result is compared with that by the standard quantum annealing (QA) using qubits. We find that the performance of the BQA is comparable to the standard QA, or gives better results in some cases.

1. Introduction

Quantum annealing (QA) is a heuristic method for solving optimization problems.[1,2] It is a kind of adiabatic quantum optimization algorithms[3–6] and is used for a device manufactured by D-Wave Systems.[7,8]

In the standard QA, the problem part of the Hamiltonian is represented by an Ising-spin model and the quantum fluctuations are induced by a transverse-field term. The corresponding Hamiltonian is familiar in statistical mechanics and is used as a standard model for quantum phase transitions.[9]

The transverse field is not the only possible way of controlling the adiabatic state and we can find many other choices in principle. In fact, it has been recognized that "nonstoquastic" effect improves the performance.[10–13] Although it is an interesting problem to find an efficient driver term from a theoretical point of view, the implementation of the complicated form of the Hamiltonian in laboratory is a difficult problem.

It is also an interesting problem to study other possible mechanisms utilizing quantum effects. In this paper, we propose and study a bifurcation-based QA (BQA) by using a spin model. The bifurcation mechanism was proposed in a parametrically driven Kerr nonlinear oscillator as a method of adiabatic quantum optimization.[14] The performance and properties of the mechanism were studied in subsequent studies.[15–20] The model is described by bosonic operators and has continuous degrees of freedom. It is an interesting problem to find the corresponding mechanism in discrete spin models, which is the main aim of this study.

The qubit operations are described by Pauli operators of spin-1/2. Since the operators are too simple to make a bifurcation, we consider a higher spin system. By referring to the standard form of the QA, we construct a spin model as a possible realization of the BQA. We show that the system can be realized in the present technology and study the performance numerically in the present work.

The organization of this paper is as follows. In Sect. 2, we introduce a spin model realizing a bifurcation and discuss a possible implementation. In Sect. 3, we numerically study the bifurcation mechanism by using a noninteracting Hamiltonian. The interactions are introduced in Sect. 4 and we compare the result with that from the standard QA. The last Sect. 5 is devoted to conclusion.

2. Bifurcation-Based Quantum Annealing

2.1 Bifurcation mechanism

The main aim of the QA is to find the ground state of the Hamiltonian

$$H_{\rm p} = -\sum_{\langle i,j\rangle} J_{ij}\sigma_i\sigma_j - \sum_{i=1}^{N} h_i\sigma_i, \tag{1}$$

for a given set of $\{J_{ij}\}$ and $\{h_i\}$. $\{\sigma_i\}_{i=1,2,\dots,N}$ represents Ising-spin variables and each spin σ_i takes $+1$ or -1. The solution, the ground-state configuration, is specified by a set of values of $\{\sigma_i\}$.

In the bifurcation mechanism, we start the time evolution from a symmetric state "$|0\rangle$" and find degenerate states "$|\pm1\rangle$" at the end of the evolution. The degenerate states represent qubit states. In the standard QA with Ising-spin variables, the degenerate states represent Ising-spin states and the initial state is given by a superposition of the Ising-spin states: $|0\rangle = (|+1\rangle + |-1\rangle)/\sqrt{2}$. To make the bifurcation, we need a bifurcation operator that gives the same eigenvalue when it acts on $|\pm1\rangle$. Since we cannot construct such an operator in Ising-spin systems, we extend the state space.

We consider the spin-1 operators $\hat{\boldsymbol{S}} = (\hat{S}^x, \hat{S}^y, \hat{S}^z)$. These operators obey the standard commutation relations such as $[\hat{S}^x, \hat{S}^y] = i\hat{S}^z$, and have the quantum number $S = 1$ when the eigenvalue of $\hat{\boldsymbol{S}}^2$ is denoted as $S(S+1)$. We use the eigenstates of $\hat{S}^z$, $|m\rangle$, as

$$\hat{S}^z|m\rangle = m|m\rangle, \tag{2}$$

with $m = +1, 0, -1$. In this basis, each operator can be represented as

$$\hat{S}^z = \begin{pmatrix} 1 & 0 & 0 \\ 0 & 0 & 0 \\ 0 & 0 & -1 \end{pmatrix}, \quad \hat{S}^x = \frac{1}{\sqrt{2}}\begin{pmatrix} 0 & 1 & 0 \\ 1 & 0 & 1 \\ 0 & 1 & 0 \end{pmatrix}. \tag{3}$$

Since we do not use $\hat{S}^y$ in the following analysis, it is omitted here. A crucial difference from the Pauli operators is that the square of each operator is not proportional to the identity operator and gives a new kind of operators:

$$(\hat{S}^z)^2 = \begin{pmatrix} 1 & 0 & 0 \\ 0 & 0 & 0 \\ 0 & 0 & 1 \end{pmatrix}, \quad (\hat{S}^x)^2 = \frac{1}{2}\begin{pmatrix} 1 & 0 & 1 \\ 0 & 2 & 0 \\ 1 & 0 & 1 \end{pmatrix}. \tag{4}$$

For a qutrit system described by the spin-1 operators, the symmetric state $|0\rangle$ is assigned to the state with $\hat{S}^z|0\rangle = 0$ and the degenerate states $|\pm1\rangle$ with $\hat{S}^z|\pm1\rangle = \pm|\pm1\rangle$. We

note that $(\hat{S}^z)^2|0\rangle = 0$ and $(\hat{S}^z)^2|\pm 1\rangle = |\pm 1\rangle$. Then, for a single qutrit i, we consider the Hamiltonian

$$\hat{H}_i(t) = -A(t)\hat{S}_i^x - B(t)(\hat{S}_i^z)^2. \tag{5}$$

We change $B(t)$ slowly from a negative large value to a positive large one. $A(t)$ is taken to be small but finite values at intermediate times so that it induces energy-level mixing. By evolving the system adiabatically with this Hamiltonian, we find that the ground state is changed from $|0\rangle$ to $|\pm 1\rangle$. In the following, we refer to the first term of Eq. (5) as driver part and the second term as bifurcation part.

We set the total Hamiltonian for N qutrits as

$$\hat{H}(t) = \sum_{i=1}^{N} \hat{H}_i(t) + \hat{H}_{\rm p}, \tag{6}$$

where $\hat{H}_{\rm p}$ represents the problem part replaced $\{\sigma_i\}$ in Eq. (1) with $\{\hat{S}_i^z\}$. We set $|B(0)| \sim |B(t_{\rm f})| \gg |J_{ij}| \sim |h_i|$ where $t_{\rm f}$ represents the annealing time. Then, each qutrit basically changes from $|0\rangle$ to $|\pm 1\rangle$. The degeneracy of the final state is lifted by the presence of $\hat{H}_{\rm p}$ and we can solve the optimization problem.

We note that the problem part, $\hat{H}_{\rm p}$, is independent of t. When $B(0)$ is a negative large number and $A(0)$ is negligible, the initial state is given by the eigenstate of $\hat{S}_i^z$ with the eigenvalue 0. The problem part only gives a zero contribution and does not affect the state even if we keep $\hat{H}_{\rm p}$ from the beginning. This is one of advantages of the present method. The time dependence of the Hamiltonian is only on each spin, $\hat{H}_i(t)$, and we do not need to change the intricate problem part, $\hat{H}_{\rm p}$. Then, it is expected that the dynamical property is basically determined by the driver and bifurcation parts and is insensitive to the problem part. This property is basically the same as that in the Kerr parametric oscillator model.[14] By using the Hamiltonian in Eq. (6), we can study the bifurcation mechanism in systems with finite Hilbert space.

2.2 *Spin coupling by nesting*

One of promising methods realizing the qutrit is to use spin nesting. The sum of two qubits gives

$$\hat{\boldsymbol{S}}_i = \frac{1}{2}(\hat{\boldsymbol{\sigma}}_{i_1} + \hat{\boldsymbol{\sigma}}_{i_2}), \tag{7}$$

where $\hat{\boldsymbol{\sigma}} = (\hat{\sigma}^x, \hat{\sigma}^y, \hat{\sigma}^z)$ represents the set of Pauli operators. As described in a standard text book on quantum mechanics, the set of operators $\hat{\boldsymbol{S}}_i = (\hat{S}_i^x, \hat{S}_i^y, \hat{S}_i^z)$ satisfies the standard commutation relations such as $[\hat{S}_i^x, \hat{S}_i^y] = i\hat{S}_i^z$ and the eigenvalues of the operator $\hat{\boldsymbol{S}}_i^2$ are denoted by $S(S+1)$ with $S = 0$ or 1. $\hat{\boldsymbol{S}}_i^2$ commutes with each component of $\hat{\boldsymbol{S}}_i$, which means that the Hamiltonian with the operators $\hat{\boldsymbol{S}}_i$ is block-diagonalized in the eigenstate basis of $\hat{\boldsymbol{S}}_i^2$ and $\hat{S}_i^z$. When we set the initial state as an eigenstate with $S = 1$, the state of the system is described by qutrit, three of four states.

The connectivity of two qutrits is specified in Fig. 1. A single logical qutrit is made from two physical qubits. The driving represented by B is achieved by operating the interaction between physical qubits within a single qutrit. The interaction between two qutrits, J_{ij}, is represented by four bonds. In the case of Fig. 1, the total Hamiltonian is given by

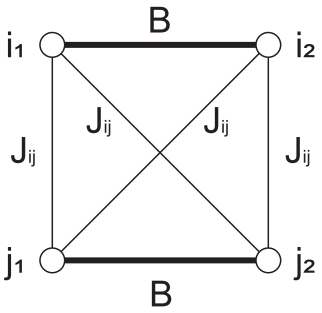

Fig. 1. The connectivity graph of two logical qutrits by four physical qubits. Logical qutrit i is made from physical qubits i_1 and i_2, and qutrit j from qubits j_1 and j_2. Two physical qubits within a single qutrit interact with each other and the interaction is controlled by $B(t)$. The interaction between two qutrits in the problem Hamiltonian, J_{ij}, is represented by four bonds. We also need additional single-qubit operations as represented by $A(t)$ (for $\sum_i \hat{\sigma}_i^x$) and h_i (for $\hat{\sigma}_{i_1}^z + \hat{\sigma}_{i_2}^z$).

$$\begin{aligned}\hat{H}(t) = &-\frac{A(t)}{2}(\hat{\sigma}_{i1}^x + \hat{\sigma}_{i2}^x + \hat{\sigma}_{j1}^x + \hat{\sigma}_{j2}^x)\\ &-\frac{B(t)}{4}[(\hat{\sigma}_{i1}^z + \hat{\sigma}_{i2}^z)^2 + (\hat{\sigma}_{j1}^z + \hat{\sigma}_{j2}^z)^2]\\ &-\frac{J_{ij}}{4}(\hat{\sigma}_{i1}^z + \hat{\sigma}_{i2}^z)(\hat{\sigma}_{j1}^z + \hat{\sigma}_{j2}^z)\\ &-\frac{h_i}{2}(\hat{\sigma}_{i1}^z + \hat{\sigma}_{i2}^z) - \frac{h_j}{2}(\hat{\sigma}_{j1}^z + \hat{\sigma}_{j2}^z).\end{aligned} \tag{8}$$

It is interesting to find that the present method is equivalent to nesting for an error-proofing procedure.[21–23] It is expected that the nested qubit can be robust against noise due to the ferromagnetic coupling between the physical qubits. In our choice of the Hamiltonian in Eq. (6), $\hat{S}_i^x$ changes the states $|\pm 1\rangle_i$ to $|0\rangle_i$ and there is no direct transition between $|+1\rangle_i$ and $|-1\rangle_i$. Since the energy level of the state $|0\rangle_i$ becomes large at large t, quantum fluctuations represented by virtual transitions to different levels are suppressed, which might be related to an error-proofing property. We note that the behavior can be changed by introducing additional driver terms. For example, $(\hat{S}_i^x)^2$ gives a direct coupling between $|+1\rangle_i$ and $|-1\rangle_i$. We see from Eq. (4) that $(\hat{S}^x)^2$ is equivalent to $\hat{\sigma}^x$ if the Hilbert space is effectively restricted to $m = \pm 1$.

We note that the initial state for each qutrit is given by $|0\rangle_i$ with $\hat{S}_i^z|0\rangle_i = 0$. It can be written by qubit states as

$$|0\rangle_i = \frac{1}{\sqrt{2}}(|+1/2\rangle_{i_1} \otimes |-1/2\rangle_{i_2} + |-1/2\rangle_{i_1} \otimes |+1/2\rangle_{i_2}). \tag{9}$$

$|\pm 1/2\rangle$ represent two qubit states. Although this is an entangled state and cannot be obtained by a single qubit operation, the manipulation is only for two qubits and can be obtained, e.g., by the standard QA procedure. We know various ways of controlling systems with a small number of spins and it is expected that the state can be prepared efficiently.

3. Noninteracting Systems

We study the performance of the BQA by solving the Schrödinger equation numerically. In this section, we treat noninteracting systems to confirm that the bifurcation mechanism works efficiently. Each qutrit can be treated independently and the mechanism can be studied by the single qutrit Hamiltonian

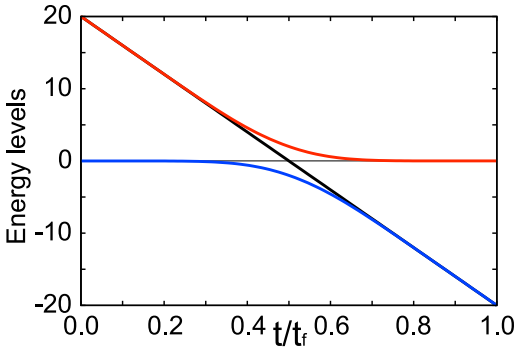

Fig. 2. (Color online) The instantaneous energy levels of the Hamiltonian in Eq. (10). We use Eqs. (11) and (12), and take $B_0/A_0 = 20$. The energy levels are plotted in unit of A_0.

$$\hat{H}(t) = -A(t)\hat{S}^x - B(t)(\hat{S}^z)^2. \tag{10}$$

We use the linear protocol for $B(t)$:

$$B(t) = B_0\left(2\frac{t}{t_\mathrm{f}} - 1\right), \tag{11}$$

where B_0 is a positive constant much larger than $A(t)$. Since our method is based on adiabaticity, we take t_f to be a large value. As we mentioned in the previous section, $A(t)$ takes small but finite values at intermediate times. We use the Gaussian protocol

$$A(t) = A_0 \exp\left[-\frac{1}{2\sigma^2}\left(2\frac{t}{t_\mathrm{f}} - 1\right)^2\right], \tag{12}$$

with $\sigma^2 = 0.1$. The instantaneous energy levels of the Hamiltonian in Eq. (10) are plotted in Fig. 2. The energy gap between the ground state and the excited state at $t = 0$ is very large. After passing through avoided-crossing region around $t/t_\mathrm{f} = 0.5$, the system has the ground state with two-fold degeneracy.

There is no guiding principle on the choice of $A(t)$. In the following, we also examine the case when $A(t)$ takes a constant value because the time-independent protocol is practically convenient. Although $A(0)$ must be zero so that the state becomes an eigenstate of $\hat{S}^z$ at $t = 0$, it is enough provided $|B(0)| \gg |A(0)|$ is satisfied.

We numerically solve the Schrödinger equation with the Hamiltonian in Eq. (10) to obtain the time-evolved state $|\psi(t)\rangle$. We first use the Gaussian protocol in Eq. (12). In Fig. 3, we plot the time dependence of probabilities $|\langle m|\psi(t)\rangle|^2$ with $m = +1, 0, -1$ for a given t_f, and the annealing-time dependence of $|\langle m|\psi(t_\mathrm{f})\rangle|^2$. We see that the bifurcation mechanism works very well if the annealing time is not considerably small. The final state is given by $(|+1\rangle + |-1\rangle)/\sqrt{2}$ and has components of $m = \pm 1$ with equal probability.

We consider the case where $A(t)$ is constant: $A(t) = A_0$. We plot the result in Fig. 4. Although we see small oscillations, the performance is almost the same as that in Fig. 3. We also examined several other cases and found similar results. This implies robustness of the bifurcation mechanism.

Next, we incorporate the noninteracting part of $\hat{H}_\mathrm{p}$. We put $J_{ij} = 0$, which means that we still have a noninteracting system and the single qutrit Hamiltonian is given by

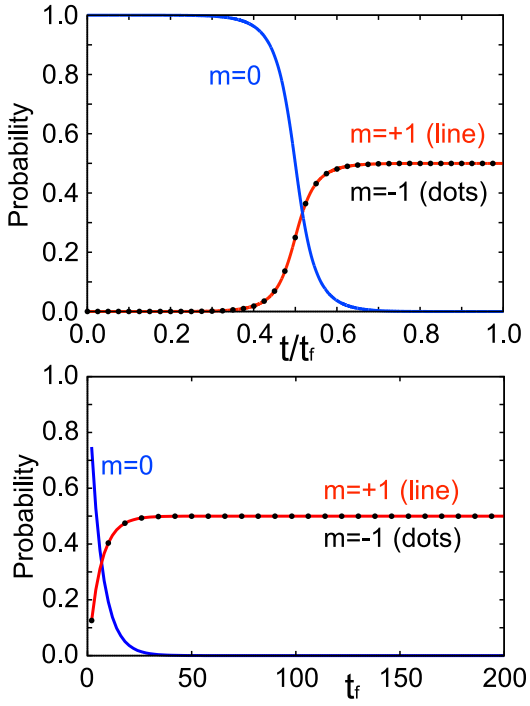

Fig. 3. (Color online) The solution of the Schrödinger equation with the Hamiltonian in Eq. (10). We use the protocol in Eqs. (11) and (12), and take $B_0/A_0 = 20$. Top: The probability distributions of the time-evolved state at each t. We take the annealing time as $A_0 t_\mathrm{f} = 100$. Bottom: The annealing-time dependence of the final state. Here, t_f is plotted in unit of A_0.

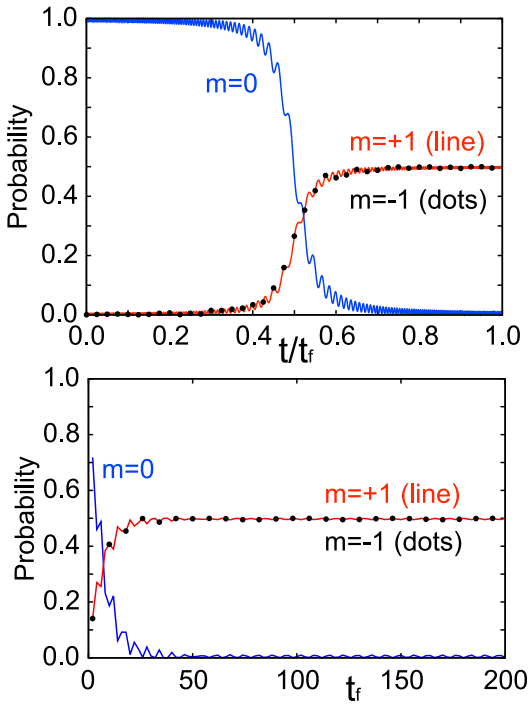

Fig. 4. (Color online) The solution of the Schrödinger equation with the Hamiltonian in Eq. (10). We take $A(t) = A_0 = \text{const}$. The other parameters are the same as those in Fig. 3.

$$\hat{H}(t) = -A(t)\hat{S}^x - B(t)(\hat{S}^z)^2 - h\hat{S}^z, \tag{13}$$

where h represents the magnetic field. The final result is determined by the sign of h.

The result is plotted in Fig. 5. We see that that the proper state, $m = +1$ or -1, is selected as a function of h, if $|h|$ is not too small.

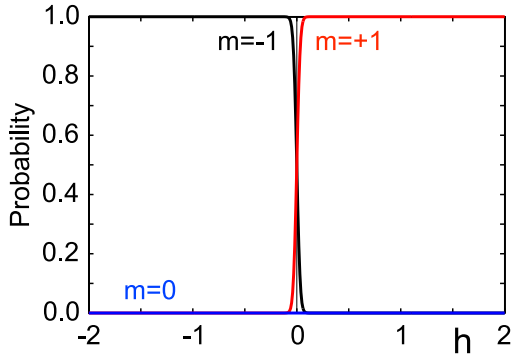

Fig. 5. (Color online) The performance with the Hamiltonian in Eq. (13). We use Eqs. (11) and (12) with $B_0/A_0 = 20$, and take the annealing time as $A_0 t_f = 200$. Each curve represents the probability of the component m at $t = t_f$. Here, h is plotted in unit of A_0.

4. Interacting Systems

Having confirmed that the bifurcation mechanism works well for a single qutrit, we study multi qutrit systems with interactions.

4.1 *Ferromagnetic interactions*

We first consider ferromagnetic interactions for a one-dimensional arrangement of spins with periodic boundary condition. Each spin interacts with the neighboring spins and we set $J_{1,2} = J_{2,3} = \cdots = J_{N,1} = J > 0$ and $h_i/J = 0.1$. Here, we introduce a finite h_i to avoid degenerate ground states. The effect of degeneracy is discussed in the next subsection.

To assess the performance of the BQA, we compare the result with that of the standard QA:

$$\hat{H}(t) = \left(1 - \frac{t}{t_f}\right)\left(-\Gamma \sum_{i=1}^{N} \hat{\sigma}_i^x\right) + \frac{t}{t_f}\left(-\sum_{\langle i,j\rangle} J_{ij}\hat{\sigma}_i^z\hat{\sigma}_j^z - \sum_{i=1}^{N} h_i\hat{\sigma}_i^z\right). \quad (14)$$

Each element is represented by qubit and the standard linear protocol is used to control the system.

The numerical result is plotted in Fig. 6. We see that, in our choice of the parameters, the computation works very well. In contrast to the standard QA, the initial state with $m = 0$ is changed to the final one abruptly after t exceeds $t_f/2$. When t is much smaller than $t_f/2$, the bifurcation part is the dominant contribution and the state remains the zero state. After passing through the region where the driver part is dominant, the state is changed to the ground state of $\hat{H}_p$.

Comparison between the QA and the BQA in the bottom panel of Fig. 6 shows that a large annealing time is required to obtain the ideal result in the case of the BQA. In the present implementation of the QA,[7,8] the scale of the Hamiltonian is of the order of GHz, and the annealing time is of the order of μs. This corresponds to $Jt_f \sim 1000$ in our unit, which is large enough to find the ideal result.

4.2 *(Un-)Fair sampling property*

In the previous example, we used a problem Hamiltonian with no ground-state degeneracy. The standard QA is known to give a biased sampling among the degenerate ground states[24,25] and we study this property in the BQA.

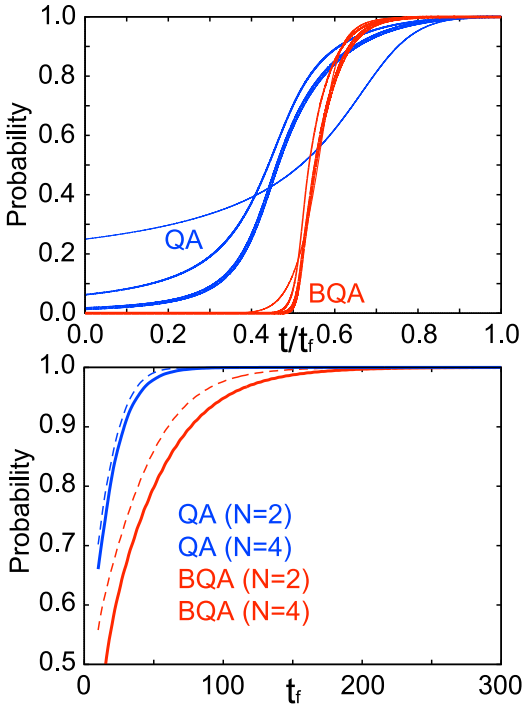

Fig. 6. (Color online) The performance with the ferromagnetic problem Hamiltonian specified in the text. For the BQA, we use the protocol in Eqs. (11) and (12) with $B_0/J = 20$ and $A_0/J = 2$. For the QA, we use Eq. (14) with $\Gamma/J = 1$. Top: The time dependence of the ground-state probability. We plot the results at $N = 2$ (thin line), 4, and 6 (thick line), each being distinguished by the thickness of the line. We take the annealing time as $Jt_f = 300$. Bottom: The annealing-time dependence. Here, t_f is plotted in unit of J.

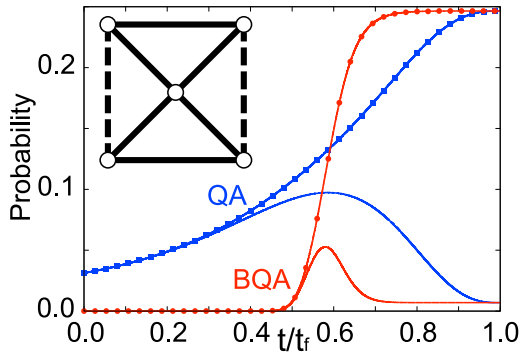

Fig. 7. (Color online) (Un-)Fair sampling properties of the QA and BQA. We use a five spin model with six degenerate ground states. The connectivity is specified in the inset where solid lines represent ferromagnetic interaction ($J_{ij} = J > 0$) and dashed lines antiferromagnetic interaction ($-J < 0$). We plot three of six states. Two of them are plotted by solid lines and the other is plotted by dotted line. The blue lines are for QA and the red for BQA. We take the annealing time as $Jt_f = 300$.

We use a five spin model used in a previous work[24] which is denoted in the inset of Fig. 7. This system has six ground states. Half of them are due to spin-flip symmetry and we plot three levels in Fig. 7. We see that the result of the BQA is very similar to that of the QA. Two of three levels are equally sampled and the other single level is suppressed. We checked that this property is unchanged when we use several different protocols.

As discussed in the original study,[24] we can improve the result by introducing additional driver terms to the Hamiltonian. Since the present model has a larger Hilbert

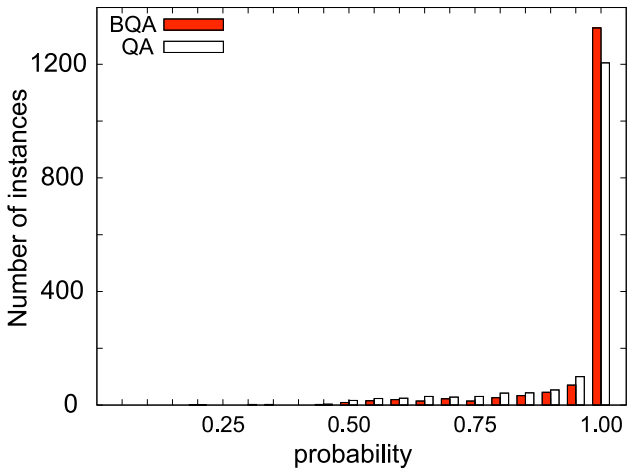

Fig. 8. (Color online) Histograms for the success probability for random Hamiltonians with $N = 4$. We compare the results of the BQA and QA. We take the annealing time as $Jt_f = 300$ and the number of samples is 1600. The bin width of the histogram is 0.05.

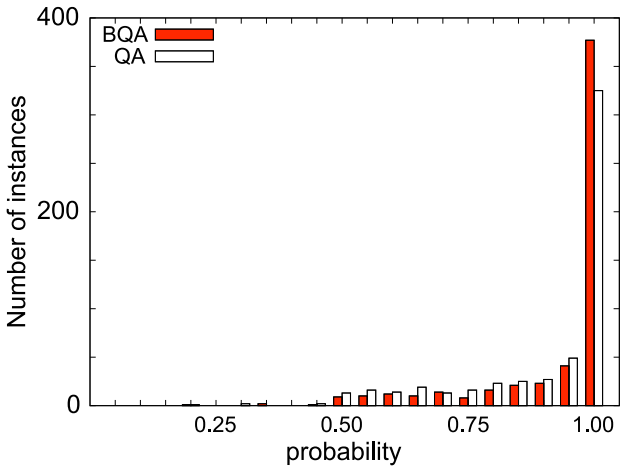

Fig. 9. (Color online) The result for the case where the ground-state configuration is nontrivial. The calculation conditions are the same as those in Fig. 8. The number of samples is 545.

space, we have many choices to improve the result, in principle. It is an interesting problem, but is beyond the scope of the present study.

4.3 Random interactions

We study random systems where J_{ij} and h_i are chosen randomly. We treat a fully-connected model with $J_{ij} = r_{ij}/N$ $(i \neq j)$, and r_{ij} and h_i are sampled from uniform distribution $[-J, J]$.

We show the result in Fig. 8. We see that the BQA outperforms the QA, though we cannot find a drastic change. We checked in the result of the BQA that the obtained state does not include the zero state $|0\rangle_i$, which means that the bifurcation works well.

To see that the method works even if the solution of the problem is nontrivial, we plot in Fig. 9 the result for samples in which the ground-state configurations $\{S_i\}_{i=1,\ldots,N}$ are not equal to $\{\mathrm{sign}(h_i)\}_{i=1,\ldots,N}$. We still find that the BQA gives a better result than the QA.

4.4 First-order phase transition for large systems

It is hard to obtain numerical results for large values of N in the present method. Instead, we study statistical properties at thermodynamic limit $N \to \infty$ by using the mean-field approximation.

The statistical mechanical model of the present type of the Hamiltonian has been discussed in various works as a model to describe λ transition in mixtures of He^3 and He^4.[26–29] In the mean-field approximation for ferromagnetic systems without magnetic field, the system is described by effective Hamiltonian

$$\hat{H}_{\mathrm{eff}}(m_s) = -A\hat{S}^x - B(\hat{S}^z)^2 - Jzm_s\hat{S}^z, \tag{15}$$

where z represents the coordination number, the number of couplings of a single spin to the other spins, and m_s is the magnetization determined selfconsistently. The selfconsistent equation is written as

$$m_s = \langle\psi_{\mathrm{GS}}(m_s)|\hat{S}^z|\psi_{\mathrm{GS}}(m_s)\rangle, \tag{16}$$

where $|\psi_{\mathrm{GS}}(m_s)\rangle$ is the ground state of $\hat{H}_{\mathrm{eff}}(m_s)$.

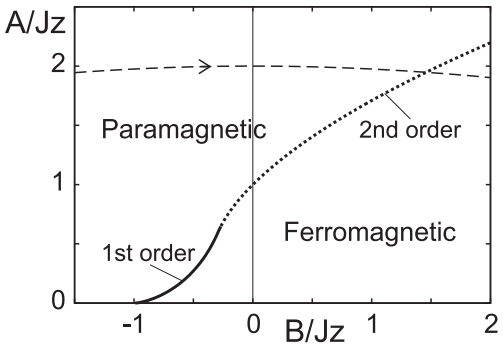

Fig. 10. The phase diagram of the ferromagnetic model in the mean-field approximation. The paramagnetic phase ($m_s = 0$) and ferromagnetic phase ($m_s > 0$) are separated by first-order and second-order phase-transition lines. The dashed line with arrow represents the protocol $(A(t), B(t))$ used in this study.

The selfconsistent equation always has the paramagnetic solution $m_s = 0$. The ferromagnetic solutions with $m_s > 0$ are obtained in a certain range of parameters as we show in Fig. 10. Those two phases are separated by a phase transition. It is of second order when the order parameter m_s changes continuously and of first order when m_s changes discontinuously. The first-order phase transitions occur when $|A|$ is small and B is negative. At the first-order transition, the zero state $m = 0$ is changed discontinuously to the qubit states. We note that the paramagnetic phase with $m_s = 0$ does not distinguish between the zero state $m = 0$ and the Ising paramagnetic state, mixtures of $m = \pm 1$. The zero state is dominant when B is negative and the Ising paramagnetic state is dominant when B is positive.

Since the first-order transition is between the zero state and the qubit states, this property is mainly determined by competing effects between the driver part and the bifurcation part and is insensitive on the details of the problem part. In fact, we can also find a similar behavior when we treat random systems.[29] We still find a first-order transition at small $|A|$ and negative B with the ferromagnetic phase replaced by the spin-glass phase.

It is known that the QA fails when the system goes across the first-order phase boundary.[30] To avoid the first-order

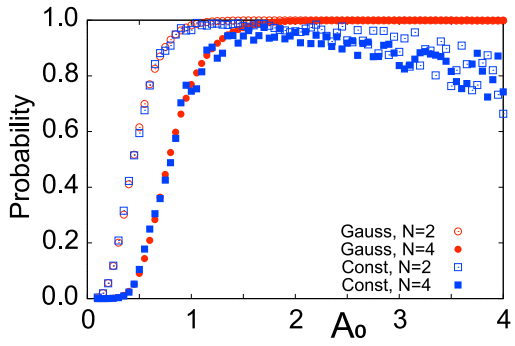

Fig. 11. (Color online) A_0 dependence of the result. We study the ferromagnetic model treated in Fig. 6. "Gauss" represents the protocol $A(t)$ in Eq. (12) and "Const" represents $A(t) = A_0$. A_0 is plotted in unit of J.

transition in the BQA, A must be taken to be a large value. We study a ferromagnetic model to see how the result is dependent on the choice of A_0. The result is plotted in Fig. 11. The computation fails when A_0 is small as we expect from the phase diagram in Fig. 10. The statistical mechanical analysis shows that the failure at small A_0 is restricted to a finite range of the parameter even if we consider large N.

5. Conclusion

We have discussed the bifurcation mechanism by using a spin model. The model can be constructed from the standard qubit system by nesting. We found in our numerical calculation that the performance of the BQA is better than that of the QA. Although we did not find a drastic change, the result can be further improved by optimizing protocols, driver part, and some other parameters.

Compared with the standard QA, our method has several different properties. First, the problem part of the Hamiltonian is independent of time and is convenient for implementations. We can only control the driver and bifurcation parts which are common to any process. Since the dynamics is mainly determined by those parts, we can study optimizations of the protocol by using the single qutrit Hamiltonian.

Second, our Hamiltonian forbids direct transition between qubit states $m = \pm 1$. Their states are only interchanged by way of the zero state. It is considered to give an error-proofing property.

Third, the model uses an extended Hilbert space and we can in principle introduce different types of operators to enhance the performance. We must be careful when we introduce a new operator since it can affect the second property we mentioned above.

Admittedly, the present study is limited to small spin systems and it is difficult to draw firm conclusions on the performance of the BQA. However, we stress that studying a different mechanism of adiabatic quantum optimization algorithms is an important problem to obtain a better understanding of quantum computations. We expect that the mechanism discussed in this paper brings a new direction of research.

Acknowledgment The author is grateful to Takuya Hatomura for useful comments. This work was supported by JSPS KAKENHI Grants Nos. JP20K03781 and JP20H01827.

1) T. Kadowaki and H. Nishimori, Phys. Rev. E **58**, 5355 (1998).
2) J. Brooke, D. Bitko, T. F. Rosenbaum, and G. Aeppli, Science **284**, 779 (1999).
3) E. Farhi, J. Goldstone, S. Gutmann, and M. Sipser, arXiv:quant-ph/0001106.
4) E. Farhi, J. Goldstone, S. Gutmann, J. Lapan, A. Lundgren, and D. Preda, Science **292**, 472 (2001).
5) A. Das and B. K. Chakrabarti, Rev. Mod. Phys. **80**, 1061 (2008).
6) T. Albash and D. A. Lidar, Rev. Mod. Phys. **90**, 015002 (2018).
7) M. W. Johnson, M. H. S. Amin, S. Gildert, T. Lanting, F. Hamze, N. Dickson, R. Harris, A. J. Berkley, J. Johansson, P. Bunyk, E. M. Chapple, C. Enderud, J. P. Hilton, K. Karimi, E. Ladizinsky, N. Ladizinsky, T. Oh, I. Perminov, C. Rich, M. C. Thom, E. Tolkacheva, C. J. S. Truncik, S. Uchaikin, J. Wang, B. Wilson, and G. Rose, Nature **473**, 194 (2011).
8) S. Boixo, T. F. Rønnow, S. V. Isakov, Z. Wang, D. Wecker, D. A. Lidar, J. M. Martinis, and M. Troyer, Nat. Phys. **10**, 218 (2014).
9) S. Suzuki, J. Inoue, and B. K. Chakrabarti, *Quantum Ising Phases and Transitions in Transverse Ising Models* (Springer, Heidelberg, 2013) 2nd ed.
10) E. Farhi, J. Goldstone, and S. Gutmann, arXiv:quant-ph/0208135.
11) S. Bravyi, D. P. DiVincenzo, R. Oliveira, and B. M. Terhal, Quantum Inf. Comput. **8**, 361 (2008).
12) Y. Seki and H. Nishimori, Phys. Rev. E **85**, 051112 (2012).
13) E. Crosson, E. Farhi, C. Y.-Y. Lin, H.-H. Lin, and P. Shor, arXiv:1401.7320.
14) H. Goto, Sci. Rep. **6**, 21686 (2016).
15) H. Goto, Phys. Rev. A **93**, 050301(R) (2016).
16) H. Goto, Z. Lin, and Y. Nakamura, Sci. Rep. **8**, 7154 (2018).
17) H. Goto, J. Phys. Soc. Jpn. **88**, 061015 (2019).
18) H. Goto, K. Tatsumura, and A. R. Dixon, Sci. Adv. **5**, eaav2372 (2019).
19) S. Masuda, T. Ishikawa, Y. Matsuzaki, and S. Kawabata, Sci. Rep. **11**, 11459 (2021).
20) S. Masuda, A. Yamaguchi, T. Yamaji, T. Yamamoto, T. Ishikawa, Y. Matsuzaki, and S. Kawabata, New J. Phys. **23**, 093023 (2021).
21) S. Matsuura, H. Nishimori, T. Albash, and D. A. Lidar, Phys. Rev. Lett. **116**, 220501 (2016).
22) S. Matsuura, H. Nishimori, W. Vinci, T. Albash, and D. A. Lidar, Phys. Rev. A **95**, 022308 (2017).
23) S. Matsuura, J. Phys. Soc. Jpn. **88**, 061006 (2019).
24) Y. Matsuda, H. Nishimori, and H. G. Katzgraber, New J. Phys. **11**, 073021 (2009).
25) M. S. Könz, G. Mazzola, A. J. Ochoa, H. G. Katzgraber, and M. Troyer, Phys. Rev. A **100**, 030303(R) (2019).
26) M. Blume, Phys. Rev. **141**, 517 (1966).
27) H. W. Capel, Physica **32**, 966 (1966).
28) M. Blume, V. J. Emery, and R. B. Griffiths, Phys. Rev. A **4**, 1071 (1971).
29) S. K. Ghatak and D. Sherrington, J. Phys. C **10**, 3149 (1977).
30) T. Jörg, F. Krzakala, J. Kurchan, A. C. Maggs, and J. Pujos, Europhys. Lett. **89**, 40004 (2010).